Supplemental Material

Quantifying carbon site switching dynamics in GaN by electron holography

K. Ji[1], M. Schnedler[1], Q. Lan[1], J.-F. Carlin[2], R. Butté[2], N. Grandjean[2], R. E. Dunin-Borkowski[1], and Ph. Ebert[1]

1) Ernst Ruska Centrum (ER-C-1) and Peter Grünberg Institut (PGI-5), Forschungszentrum Jülich GmbH, 52425 Jülich, Germany

2) Institute of Physics, Ecole Polytechnique Fédérale de Lausanne, 1015 Lausanne, Switzerland

1. TEM lamella preparation by FIB

Prior to thinning, the bulk semiconductor sample was coated with a C protective layer. The lamella was initially thinned to 1700 nm using a ±2° tilt relative to the incoming Ga^+ beam at 30 kV and 0.77 nA. Further thinning proceeded with currents of 0.4 nA and 0.24 nA at ±1.5° tilt until a thickness of approximately 500 nm was reached. The final thinning stage involved a low beam current of 83 pA at 30 kV with a ±1.2° tilt, followed by a polishing process established at 5 kV and with a 16 pA with a ±5° tilt.

2. Lamella thickness

The overall thickness of lamella was measured with the secondary electron microscope integrated inside the FIB system. The crystalline thickness was measured with convergent beam electron diffraction. The thickness of amorphous layer is determined by subtracting the overall thickness with the crystalline one. The thickness information of lamellas subjected under different annealing temperatures are summarized in Tab. S1 below.

Annealing temperature [°C]	Crystalline thickness [nm]	Overall thickness [nm]	Amorphous layer thickness [nm]
360	362 ± 5	380 ± 10	9.0 ± 5.6
390	344 ± 6	363 ± 10	9.5 ± 5.8
420	341 ± 5	360 ± 10	9.5 ± 5.6
450	361 ± 8	375 ± 10	7.0 ± 6.4

Table S1: *Thicknesses information of TEM lamellas used in this work.*

3. Off-axis electron holography experimental details

The upper biprism is used and biased at 70 V as a trade-off between a proper field-of-view and a high contrast of the interference patterns. The lamella is kept at edge-on orientation and tilted away from the $[10\bar{1}0]$ zone axis to minimize the contrast from the dynamical diffraction. After a certain annealing time, single-frame holograms are acquired at room temperature with an exposure time of 10–12 s. To improve the signal-to-noise ratio, a minimum number of two holograms are averaged together for subsequent data analysis and processing. The phase profile is extracted from region free of dynamic diffraction contrast.

Examples of dynamic-contrast-free phase and amplitude maps acquired at 360 °C for the as FIB-prepared and healed lamella are depicted in Fig. S1.

Examples of phase profiles acquired for annealing temperatures of 390 °C, 450 °C, and 490 °C are illustrated in Fig. S2 (a), (b), and (c), respectively. The additionally shown measurement at 490 °C has not been included in the analysis, since the time constant is significantly smaller than the smallest annealing time possible. It is only shown for completeness here.

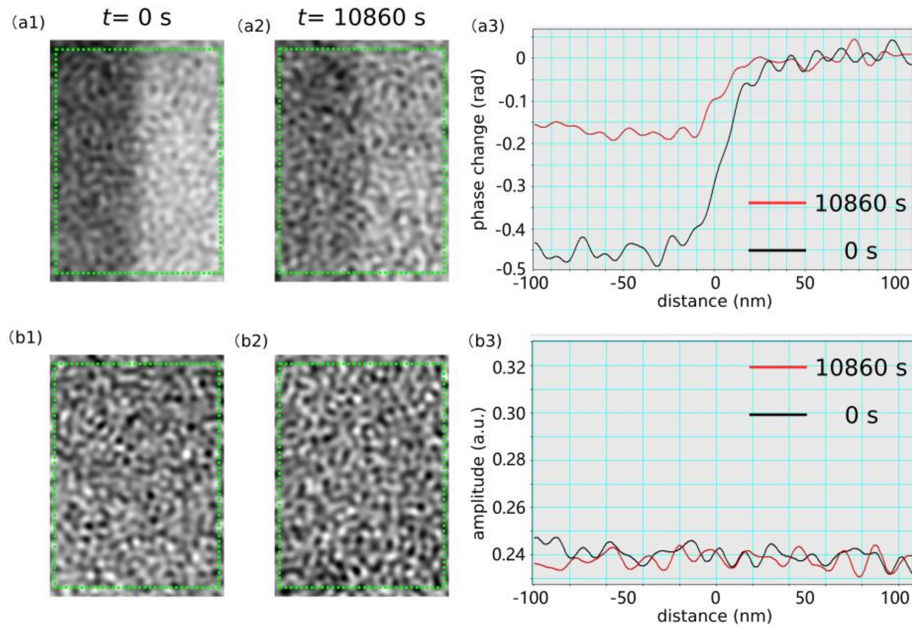

***Figure S1**: (a1, a2) Single-frame phase maps acquired at as FIB-prepared state (i.e., without annealing) and healed state (i.e., 10860 s under 360°C) lamella. The line profiles extracted from the green rectangles are depicted in (a3). (b1, b2) Corresponding amplitude maps. (b3) Line profiles of amplitude are flat across the n-n⁺ GaN junction, suggesting the absence of dynamic diffraction.*

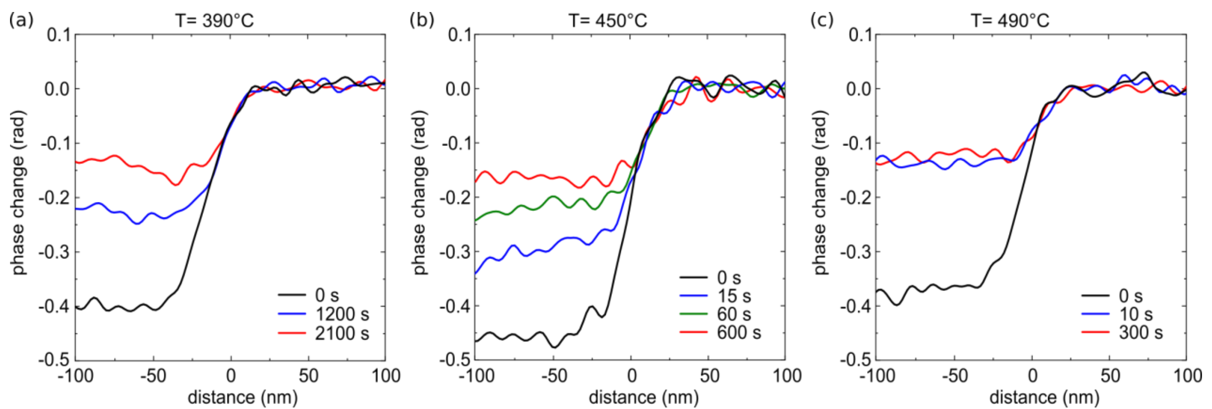

***Figure S2**: Temporal evolution of phase profiles extracted from phase maps obtained at annealing temperatures of (a) 390°C, (b) 450°C, and (c) 490°C.*

4. Influence of electron beam irradiation

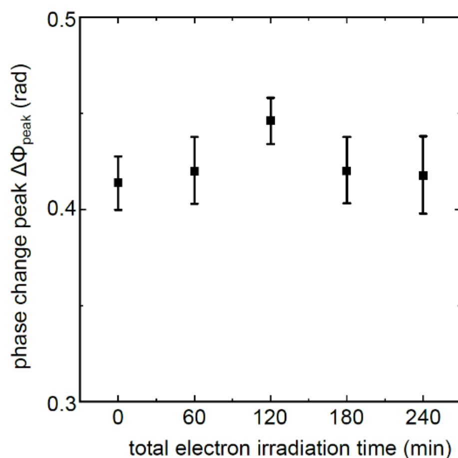

***Figure S3:** Phase contrast across the n-n⁺ doping junction versus electron irradiation exposure time for a dose rate of 30 e/nm² s. No change is detectable for up to at least 4 hours irradiation, demonstrating that the electron beam does not affect the derived electrostatic potential under the used experimental conditions. Note, during annealing the gun valve is closed and no e-beam irradiation takes place.*

5. TRIM simulation of C distribution in the lamella resulting from FIB preparation

The C implantation profile into the GaN lamella was systematically simulated and derived from the Transport and Range of Ions in Matter (TRIM) simulations.[Ziegler:2010] Even in much better vacuum environments than that used in the FIB, it is well known that predominantly carbon contaminates the surfaces of samples. In addition, carbon is used as protective layers in the FIB, enhancing carbon contaminations. Therefore, we modelled the situation in the FIB using TRIM simulations of a 2 nm thick carbon contamination layer on top of GaN. Note, the thickness of the carbon layer does not represent the much thicker carbon protection layer deposited on the sample before lamella cutting, but resembles a thin C film that is permanently deposited on the lamella by the electron beam and residual C in the FIB chamber. For the Ga^+ ion beam, we used the same incident angle (5°) and energy (5 kV) as well as our used ion dose rate (16 pA) of the very last polishing step of the lamella in FIB (see section 1 above). The TRIM results in Fig. S4 demonstrate that carbon is recoiled sufficiently deep into the subsurface region of the GaN crystal in concentrations significantly larger than the doping concentration. Hence, the recoiled C present is able to pin the Fermi level fully.

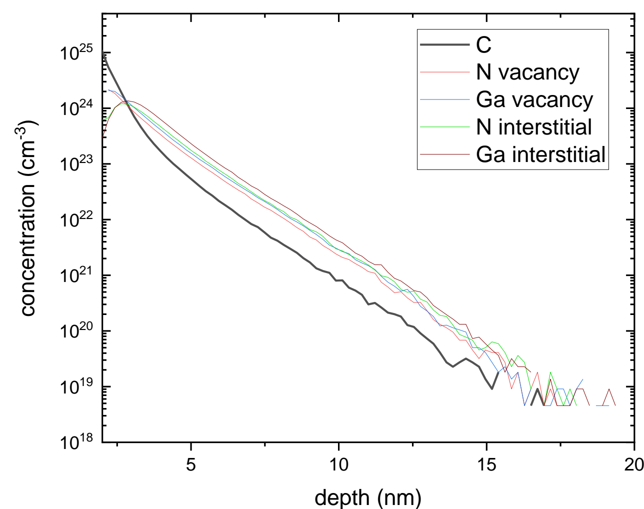

Figure S4: TRIM results of the recoil distribution of C as well as Ga and N in form of vacancies and interstitials in the GaN layer for a total of 99999 incoming Ga^+ ions at 5 kV acceleration voltage and an incident angle of 5°, as well as a carbon layer thickness of 2 nm. The thickness of the amorphous layer can be estimated on basis of the displaced atoms. At a thickness smaller than 9 nm (incl. the 2 nm C layer) more than 10% of atoms were displaced and one can anticipate that amorphization occurred certainly. This thickness is in good agreement with the measured thickness of the amorphous layer of about (9.2 ± 3.3) nm. Beyond this it is anticipated that the crystalline structure is preserved. Note, for the interpretation of the large vacancy and interstitial concentrations one needs to recall that the simulation does not consider recombination. If recombination is taken into account, most of the N and Ga vacancies will be annihilated already at room temperature in the GaN layer remaining crystalline due to the low diffusion barriers. Thus, the dominating defect will be C impurities in line with our experiments.

[Ziegler:2010] J. F. Ziegler et al., Nucl. Instrum. Methods Phys. Res. B **268**, 1818 (2010).

6. Identification of C_N as electrically dominating point defect in FIB prepared GaN lamellas

In order to identify the type of point defect leading to the Fermi level pinning one needs to consider the physics describing the charge states and changes of charge states of point defects:

n-type GaN can only be pinned by defects exhibiting a charge transfer level involving negative charge states, e.g. (0/-), in the band gap. Note, a charge transfer level involving positive charge states can only pin *p*-type, but not *n*-type materials. For defect concentrations higher than the doping concentration the Fermi level is pinned at the (0/-) charge transfer level of the defect. Thus, the measured Fermi level pinning reveals that the (0/-) charge transfer level of the pinning point defect is about 0.6 eV above the valence band edge.

This charge transfer level can be compared with theoretical calculations of intrinsic and extrinsic point defects in GaN. We summarized for this purpose the formation energy vs. Fermi level position of the different published calculations in Fig. S5.

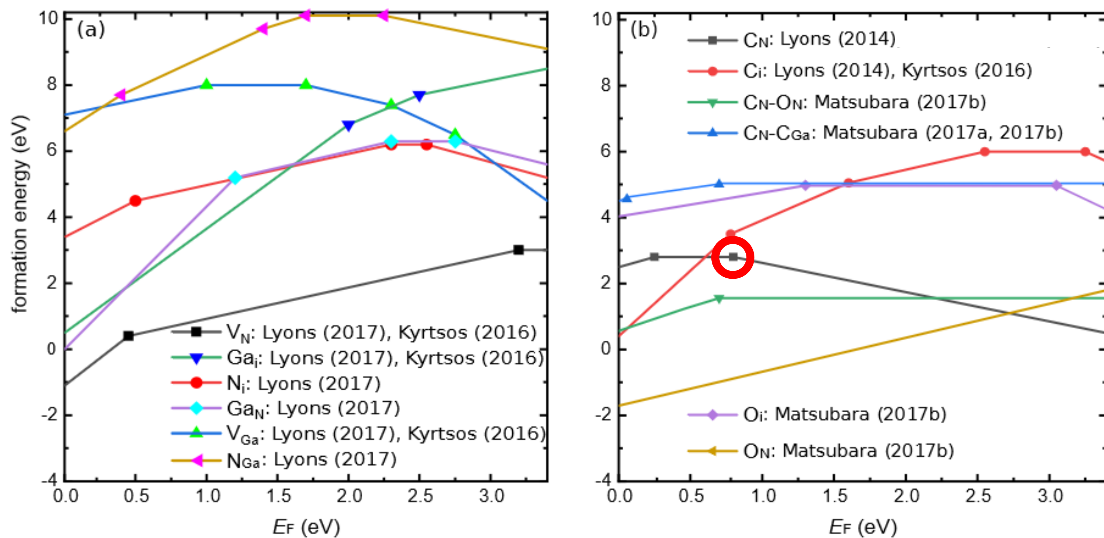

Figure S5: *(a) Formation energies of native point defects and (b) impurities as a function of the Fermi energy (relative to the valence band edge) summarized from literature. Only C_N has a (0/-) charge transfer level (red circle) in the lower part of the band gap.*

Positive (negative) slopes of the formation energies correspond to positive (negative) charge states of the defects. Uncharged states yield a horizontal line. The charge transfer levels are at the Fermi energy positions, where the curves exhibit a slope change (marked by symbols). As visible in Fig. S5a charge transfer levels involving negative charges can only be found in the upper part of the band gap for intrinsic defects. This is due to their doping compensating properties and reflects the principle of the Fermi-level stabilization energy for GaN, being in the upper part of the band gap.[Li:2005] Hence, for obtaining a (0/-) charge transfer level close to the valence band edge in the lower part of the band gap, the defect must behave in analogy to a dopant atom. This typically can only be achieved by impurities. The most common impurities are oxygen, hydrogen and carbon (nitrogen in no impurity for GaN). Oxygen acts as *n*-type dopant as visible in Fig. S5b. Hydrogen passivates *p*-type dopants and thus cannot account for the observed pinning level. Carbon incorporated substitutionally on nitrogen sites acts as (deep) acceptor in line with the need of a (0/-) charge transfer level and the calculations reveals that the (0/-) charge transfer level is about 0.8 eV above the valence band edge [Lyons:2014], in perfect agreement with the observed charge transfer level. Therefore, on basis that (i) carbon is the most common contamination amply present in FIB, (ii) carbon is implanted in large concentrations in the subsurface region of GaN under the used ion milling conditions, and (iii) carbon on nitrogen sites in the only defect exhibiting to correct type and energy of charge transfer level, we conclude that the Fermi level pinning is due to C on nitrogen sites.

This is further supported by the results of the dynamics of the healing process: The energy barrier is in perfect agreement with that calculated for a site change of carbon. In addition, the one lattice distance long diffusion length indicates a site switch from substitutional to interstitial, which is only compatible with C impurities, but not with any intrinsic point defect.

[Lyons:2014] J. L. Lyons, A. Janotti, and C. G. Van de Walle, Phys. Rev. B **89**, 035204 (2014).
[Li:2005] S. X. Li *et al.*, Phys. Rev. B **71**, 161201 (2005).
[Kyrtsos:2016] A. Kyrtsos, M. Matsubara, and E. Bellotti, Phys. Rev. B **93**, 245201 (2016).
[Matsubara:2017a] M. Matsubara and E. Bellotti, J. Appl. Phys. **121**, 195701 (2017).
[Matsubara:2017b] M. Matsubara and E. Bellotti, J. Appl. Phys. **121**, 195702 (2017).

7. Electrostatic simulation

Partial differential equations and solver scheme:
The electrostatic simulation is based on an iterative finite-difference Newton-SOR solver for both, Poisson and continuity equations in the framework of drift and diffusion equations, taking into account quantum corrections. The initial carrier concentrations are derived in the parabolic band approximation using (geometric mean) density of states effective masses and by solving the charge neutrality condition. The discretized differential equations are summarized in:
M. Schnedler, V. Portz, P. H. Weidlich, R. E. Dunin-Borkowski, and Ph. Ebert, Phys. Rev. B **91**, 235305 (2015).
M. Schnedler, R. E. Dunin-Borkowski, and Ph. Ebert, Phys. Rev. B 93, 195444 (2016).

Surface state treatment:
Surface states are modelled as two-dimensional Gaussian-shaped charge distributions, peaking at the charge transfer level of the corresponding defect. The surface states are in thermal equilibrium with the bulk material, i.e. they are filled from the charge neutrality level to the bulk Fermi level. The two-dimensional charge results in a surface potential. The surface potential is screened towards to bulk by carrier redistribution, following the Poisson and continuity equations.

Design of the mesh:
The equidistant simulation grid is given in three-dimensional Euclidean geometry with 55 node points in each spatial direction. The physical dimensions of the grid are 220 nm in *x* direction (perpendicular to the n-n^+ interface), 55 nm in *y* direction and 420 nm in *z* direction (e-beam direction). We use Neumann boundary conditions.

Design of the lamella:
The lamella is designed to have an infinite extension in *x* and *y* direction and the CBED measured crystalline thickness in *z* direction. The surface shells of the lamella are modelled as follows:

I. The amorphous shell is homogeneous throughout the whole lamella surface and thus creates an offset to the phase, which is equal on both sides of the n-n^+ interface. Since we are only interested in the phase change across the interface, the amorphous layer is not included in the simulation.
II. According to the TRIM ion recoiling simulations, the crystalline but defect rich shell, where the C concentration is between 10^{23} - 10^{18} cm^{-3}, has a thickness of approximately 5-6 nm. Since the grid spacing in *z* direction is about 8 nm, this layer is modeled using a single node-point (in *z* direction) at the surface of the FIB-prepared lamella, which exhibits a concentration of two-dimensional defect states in the order of 10^{14} cm^{-2} (equivalent to approximately a 10^{22} - 10^{23} cm^{-3} defect concentration in a 5-6 nm thick surface layer). As described above, this 2D defect density gives rise to surface Fermi-level pinning.

The GaN bulk material of the lamella is modelled using the following quantities:

Physical parameter	Value
Dielectric constant (relative to vacuum permittivity ε_0)	8.9 ε_0
Electron affinity	4.1 eV
Density of states effective mass (valence band)	1.4 m_e
Density of states effective mass (conduction band)	0.2 m_e
Band gap	3.4 eV
Acceptor concentration	0
Donor concentration	3.5×10^{18} cm^{-3} (n^+) / 7.7×10^{17} cm^{-3}(n)
Ionization energy of acceptors	n/a
Ionization energy of donors	26 meV

Table S2: *Physical parameters used for the simulation*

Derivation of phase maps:
The phase maps were derived by integration of the three dimensional electrostatic potential solution $V_E(x, y, z)$ along the z direction (beam direction), following the well-known formula

$$\theta(x,y) = C_E \int_0^w V_E(x,y,z)dz,$$

where C_E is a constant depending on the acceleration voltage and w the crystalline thickness of the lamella.

8. Cross-sectional band diagram through the simulated lamella

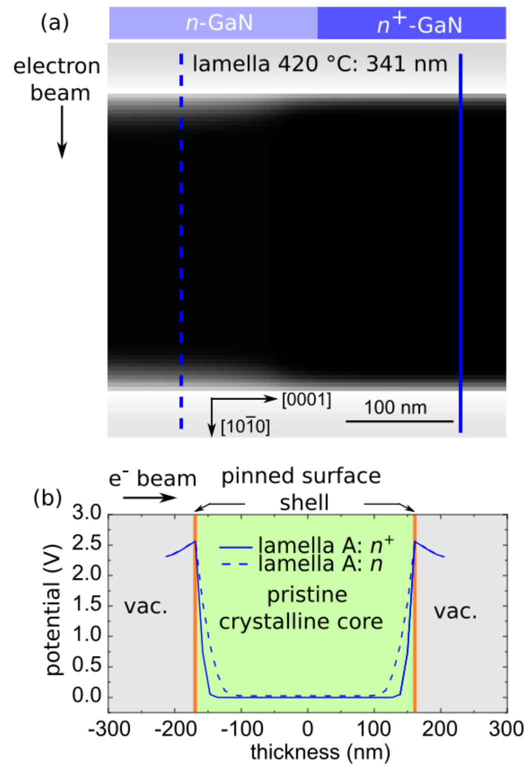

***Figure S6**: Simulated cross-sectional electrostatic potential map of the GaN n-n+ doping step for TEM lamellas with a thickness of 341 nm (a) in gray scale visualization. (b) Potential profiles extracted along the respective vertical dashed and solid lines in (a) through the n and n+ doped region for comparison. The vacuum and pristine crystalline core are visualized with gray and green background color, respectively. The calculation has been done for a crystalline thickness of 341 nm, corresponding to that of the sample annealed at 420°C (see Table S1).*